Electronic Supplementary Materials

For https://doi.org/10.1631/jzus.A2400013

Multi-field, time-varying behavior and cracking mechanisms of early-age concrete in balastless track beds

Xiao LI[1,2], Juanjuan REN[1], Xueyi LIU[1], Zeyong ZHANG[1], Shijie DENG[1]

[1]*MOE Key Laboratory of High-speed Railway Engineering, Southwest Jiaotong University, Chengdu 610031, China*
[2]*China MCC5 Group Corp. Ltd., Chengdu 610063, China*

Section S1 Introduction to Double-Block Track Structure

The double-block track structure is composed of steel rails, WJ-8 fasteners, double-block sleepers (prefabricated with C60 concrete), a track bed (cast in place with C40 concrete), and a supporting layer of C20 concrete (for subgrade and tunnel sections) or C40 reinforced base plate (for bridge sections) [1], as shown in Fig. S1. Railway line construction requires the supporting layer or base plate to be first cast in place, after which concrete is poured at the upper track bed. Prefabricated sleepers are then positioned and embedded into the track bed to complete the sleepers and the track bed. Generally, the double-block track is a partially prefabricated and partially cast-in-place structure, with concrete poured layer by layer and sleeper embedded.

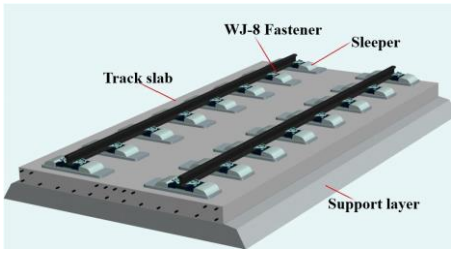

(a) Overall diagram

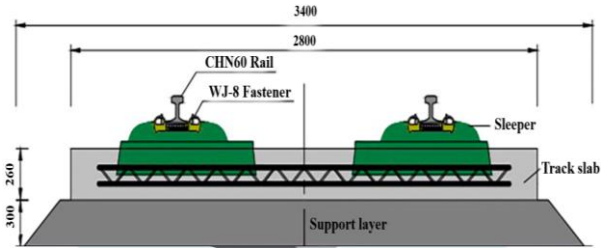

(b) Cross-sectional diagram

Fig. S1 Double-block ballastless track structure

Section S2 Research status

During research into the hydration process of cement-based materials, scholars have established a variety of hydration dynamic models through tests and experiments [2]. There are three main methods to simulate the hydration process: i). Based on the experimental research of macroscopic phenomena, empirical formulas are used to measure the influence of temperature, water-cement ratio, fineness, particle size distribution, and cement chemical composition on the hydration rate, whereby hydration is regarded as a change process of the entire cement clinker [3-5]; ii). At the macroscopic level, simulation of the integrated hydration process of clinker components or that of individual components is divided into multiple hydration stages, namely crystallization nucleation, crystal growth [6], phase boundary reaction, and diffusion [7]; iii). The CEMHYD3D [8], HydratiCA [9], HYMOSTRUC [10, 11], and μic models [12] can simulate the microscopic hydration process of cement particles during structure formation. Since the main clinker components (C3S, C2S, C3A, and C4AF) and mineral admixtures in cement have different hydration mechanisms and hydration rates, many parameters are required, such as when calculating the hydration degree of each component (at a macro level) and calculating the hydration process when cement particles form into the structure (at a micro level). Such parameters complicate model calculation and are redundant for concrete structures with strong material discreteness. Therefore, in the early hydration process of the track bed, we ignore the differences in hydration mechanism and reaction rate of various components, and instead take hydration as a whole and unified reaction process. This reduces the number of parameters needed by the model and thus alleviates the calculation workload.

Most research on the early temperature field typically ignores the thermal conductivity and specific heat capacity changes caused by hydration water consumption and environmental drying (in particular, the thermal conductivity of the newly mixed concrete, which is approximately 1.5 times that of the older dry concrete). Although most research uses constant thermal parameters when simulating the temperature field of early-age concrete [5], other work also considers the influence of hydration degree and free water content on thermal parameters [4, 13]. In addition, the traditional hydration heat-age empirical formula is suitable for calculating the temperature field of large-volume early-age concrete such as that used in gravity dams impervious to the environment. However, the concrete track bed of slab tracks is a flat structure whose early hydration heat release rate is greatly affected by ambient temperature and humidity. When researching the temperature field in complex conditions in the early age of the track bed, it is a good practice to calculate the heat of hydration through the macroscopic hydration kinetic model (temperature and humidity), while analyzing the influence of hydration degree and water content on thermal parameters.

Compared with the temperature field, the humidity field of early-age concrete is more complicated and thus more difficult to achieve high-accuracy testing and calculation. Existing studies mainly focus on the evolution process of relative humidity and the drying deformation of the humidity field. Common test methods for relative humidity evolution can be divided into two categories: i). study of different water-cement ratios and mineral admixtures on the humidity of early-age concrete in the sealed state, from which empirical formula is proposed for relative humidity

evolution under self-drying [14]; ii). monitoring the relative humidity in a dry external environment to study the nonlinear diffusion problem under the joint action of self-drying and water diffusion [15], while also exploring the effect of wind speed, temperature, humidity [16], and water evaporation inhibitor [17] on the dehydration rate of early-age concrete. Early calculation methods include the Fick diffusion model, which was commonly used to describe the relative humidity and reflect the mutual verification of the humidity state and the test results. However, since this method cannot reflect the internal free water content, it is difficult to verify the test results of the early-age concrete drying water loss rate, and cannot directly describe the evolution law of thermal conductivity and volumetric heat capacity with humidity. Therefore, in recent years, scholars have established more complex humidity diffusion models, represented by two types: i). humidity diffusion models with capillary pressure and vapor pressure as variables [4, 18]; ii). humidity calculation models that can describe the change of free water content and relative humidity [5, 19, 20], whereby the latter variable is used as the driving force for humidity transport to establish the relationship with water content. These two types of models can evaluate the relative humidity and free water content changes in early-age concrete. Experimental research has also been conducted on the drying shrinkage caused by the humidity field of early-age concrete [21, 22]. Results show the shrinkage strain caused by a 1% decrease in relative humidity is about 1×10^{-5} to 2×10^{-5}, which is equivalent to the strain caused by a temperature change of 1 ℃ [23]. In recent years, the research of Zhang et al. [23-25] on the relationship between internal humidity and shrinkage of concrete suggests that, over approximately the same temperature history, the internal relative humidity can be seen as the internal cause of both self-shrinkage and drying shrinkage of concrete. Therefore, when calculating and expressing the humidity deformation of early-age concrete, relative humidity is the preferred option.

At present, research into the stress field of early-age concrete centers on the relationship between the early mechanical parameters and the degree of hydration, as well as on the modeling of early creep. Most of the mechanical parameters are predicted by two types of models: i) prediction models represented by ACI standards [26], that is, under standard curing conditions, curing age is used as a parameter; and ii). test-based prediction models represented by the De schuters et al. [27] model, using the hydration degree as a parameter. In engineering practices, the hydration process of concrete is influenced by differences in pouring temperatures, environmental changes, and curing conditions, so prediction models that use the standard curing age as a parameter offer inadequate accuracy, whereas the development model of elastic modulus and tensile strength using the degree of hydration as a parameter shows stronger applicability. Based on the aforementioned theories and a large amount of test data, scholars have proposed various creep calculation models such as the ACI models, Model B3 [28], and Model B4 [29]. To measure the nonlinear creep effect of early-age concrete at high stress levels, scholars proposed a nonlinear function relationship between creep and stress using a uniaxial creep model under low stress [30, 31]. Other studies include the visco-elastic-plastic damage models considering the early plasticity or damage behaviors [32, 33], but these are seen as too nonlinear, making the solution of the models too difficult. To this end, Bazant [34] summarized three commonly used creep calculation methods: i). the age-adjusted effective modulus method, which is a one-step approximate method; ii). a step-by-step analysis of structural creep and shrinkage according to the principle of superposition using integral equations; and iii) the rate-type constitutive relation based on the Maxwell chain or Kelvin

chain. Bazant et al. argued that the third method provides more realistic results and has a wider application range because it considers the influence of different factors on early creep.

There are two mainstream hygro-thermo-chemo-mechanical coupling models for early-age concrete. One option, by Gawin [4], is a fully coupled model based on Schrefler's model of porous media for thermo-hydro-mechanical systems. On the basis of this model, Du [35] analyzed the influence of external loads on internal humidity; and You [36] analyzed the evolution laws of temperature, humidity, and stress in early-age concrete. The other type is the hygro-thermo-chemical model presented by Di Luzio [5] based on phenomenological models. Based on this type of model, further studies have been conducted. For example, Wei Zhou [19, 20] refined the water migration model and proposed a modified hygro-thermo-chemical model to describe the early water vapor saturation stage of the hydration reaction; Bocciarelli [37] performed reverse analysis on the sensitivity of the hygro-thermo-chemical-mechanical model and highlighted the model's robustness under different boundary conditions, like external temperature and relative humidity surrounding the concrete; and Liu [17] performed analysis into the impact of environmental conditions, structure types, and construction maintenance on the risk of concrete shrinkage and cracking. Both of the two model types can reflect the multi-field time-varying behaviors of early-age concrete, but using the first model type, the fully coupled hygro-thermo-chemo-mechanical model for porous media is deemed too difficult to apply and popularize due to its complex equations. For the convenience of analyzing the concrete track bed structure, it is advisable to use the hygro-thermo-chemo-mechanical coupling model based on the phenomenological method.

Section S3 Discussion on parameters of hydration field

$$A_{25} = B_1\left(\frac{B_2}{\alpha_u}+\alpha\right)\left(\alpha_u-\alpha\right)\exp\left(-\eta\frac{\alpha}{\alpha_u}\right) \tag{S1}$$

$$\beta_\varphi = \frac{1}{1+\left(e-e\varphi\right)^4} \tag{S2}$$

$$\beta_T = \exp\left[\frac{E_a}{R}\left(\frac{1}{T_{25}}-\frac{1}{T}\right)\right] \tag{S3}$$

where: α is the degree of hydration and A_{25} is the chemical affinity of the track bed concrete at the reference temperature of 25 ℃; B_1, B_2, and η are the hydration affinity coefficients, the parameters can be calibrated by simulating the temperature evolution during adiabatic tests, the range of values for the three parameters can be found in reference [38] as well; β_φ and β_T are the influence coefficients of humidity and temperature, respectively; e is the material constant，the constant values e=5.0~6.0 and can be generally adopted [5] ; φ is the relative humidity of the concrete; and E_a is the activation energy of the concrete, which can be found in reference [39].

Section S4 Discussion on parameters and boundary conditions of temperature field

S4.1 Discussion on parameters boundary conditions

The heat release rate caused by hydration of the track bed is expressed as:

$$\frac{\partial Q_h}{\partial t} = Q_h^{\infty} m_c \frac{\partial \alpha}{\partial t} \tag{S4}$$

where: Q_h^{∞} is the heat completely released by the hydration of 1kg cement, which depends on the components of the cement, and its value can be taken according to the weighted average value of the heat release of each component [40].

Considering the influence of hydration degree and free water content on the volumetric heat capacity of concrete [10], the equivalent volumetric heat capacity of track concrete can be expressed as:

$$\begin{aligned} (\rho C)_{eff} &= m_c (1+0.25)\alpha C_{cp} \\ &+ m_c (1-\alpha) C_c + m_a C_a + w_e C_w \end{aligned} \tag{S5}$$

where: 0.25 means that 1 kg of cement needs 0.25 kg of free water to be converted into bound water for complete hydration; m_c and m_a are the mass of cement and aggregate per cubic meter respectively; w_e is the content of free water in concrete at a specific moment during the hydration process; and C_{cp}, C_c, C_a, and C_w are the specific heat capacities of cement-based materials, unhydrated cement, aggregate, and free water, respectively.

Thermal conductivity is greatly affected by the water content, and there is a linear relationship between the hydration water consumption and the degree of hydration. This means the reduction of free water content caused by internal water consumption during concrete hydration is the prime reason for the decrease in thermal conductivity. The thermal conductivity of concrete can be expressed as:

$$\lambda = \lambda_0 \left(1 - f_w \frac{\Delta w_e}{\rho}\right) \tag{S6}$$

where: λ_0 is the thermal conductivity coefficient at the initial stage of mixing; f_w is the influence coefficient of free water content on thermal conductivity, and is typically 6.0~8.0 for ordinary concrete [41]; Δw_e is the reduced mass of free water in the unit volume of concrete compared with the content of mixing water at the current moment; and ρ is the density of early-age concrete.

4.2 Discussion on boundary conditions

Convective heat transfer: for both covered (with insulation) and uncovered track surfaces, the convective heat transfer can be treated using the third-type boundary conditions, and the surface heat flux q_v (W/m^2) is expressed as:

$$q_v = \alpha_v \left(T_a - T_{surf} \right) \tag{S7}$$

where: T_a is the ambient temperature (℃); T_{surf} is the surface temperature (℃) and a_v is the surface convective heat transfer coefficient (W/m^2·K), which is heavily affected by the wind speed v_f (m/s) for uncovered surfaces. a_v can be expressed as [42]:

$$\alpha_v = \begin{cases} 4.0v + 5.6 & v_f \le 5.0 \\ 7.15 v_f^{\,0.78} & v_f > 5.0 \end{cases} \tag{S8}$$

When the formwork or insulation layer is attached to the concrete surface, we must consider the influence of the insulation layer on the convective heat transfer coefficient. The specific calculation that takes this into consideration can be found in literature [42].

Solar radiation heat transfer: the heat flux q_s (W/m^2) when the surface is bare or covered with curing materials can be expressed as:

$$q_s = a_s Q_s \tag{S9}$$

where*:* a_s is the solar radiation absorption coefficient of the track surface, which is typically 0.5~0.6 [43]; and Q_s is the solar radiation intensity per unit area (W/m^2), which is assumed to be in pulse cosine form [42]:

$$Q_s = \begin{cases} Q_s^{\max} \cos\left(\dfrac{\pi \tau}{P_s} \right) & -P_s / 2 \le t \le P_s / 2 \\ 0 & |t| \ge P_s / 2 \end{cases} \tag{S10}$$

where: P_s is the sunshine radiation duration; Q_s^{max} is solar radiation intensity at the day's strongest sunshine radiation (W/m^2).

Radiation heat exchange: in addition to absorbing short-wave solar radiation, heat is also exchanged via long-wave radiation between the track surface and the atmospheric environment. The heat flux q_r (W/m^2) of radiation heat exchange can be expressed as:

$$q_r = \varepsilon_r \sigma_r \left(T_a^{\,4} - T_{surf}^{\,4} \right) \tag{S11}$$

where: σ_r is the Stefan-Boltzmann constant, which is taken as 5.67×10^{-8}W/(m^2·K^4); ε_r is the blackness coefficient. Note that if the track surface is covered with plastic film, which has limited long-wave transmittance, the radiation heat transfer between the surface of the track bed and the

atmospheric environment will be greatly weakened. As a result, ε_r is only 0.1~0.2 [50].

Evaporative heat dissipation: heat q_v (W/m^2) leaves the track surface due to water evaporation, and this can be expressed as:

$$q_v = h_v g_a \tag{S12}$$

where: h_v is the latent heat of water evaporation per unit mass (J/kg); g_a is the water evaporation flux on the concrete surface [kg/(m^2 s)] and can be calculated by the humidity field boundary condition formula (S15).

Section S5 Discussion on boundary conditions of humidity field

Considering the atmospheric environment that concrete is exposed to when pouring. Without moisturizing measures, the moisture exchange between the concrete and the flowing air can cause rapid evaporation, which can lead to cracking on the concrete's surface layer. This moisture exchange is mainly induced by the difference between the atmospheric pressure and the vapor pressure on the concrete's surface, where the evaporation flux g_a (kg/m^2 s) can be expressed as:

$$g_a = \beta\left(\varphi_e P_e^{sat} - \varphi_s P_s^{sat}\right) \tag{S13}$$

where: φ_e and φ_s are the relative humidity of the environment and concrete's surface (%); P_e^{sat} and P_s^{sat} are the saturated vapor pressure of the environment and concrete's surface (Pa); β is the water vapor transmission coefficient (s/m).

The water vapor transmission coefficient is mainly affected by wind speed and when exposed to atmospheric conditions can be expressed as [40]:

$$\beta = 8.7\times10^{-8}\left(0.253 + 0.216 v_f\right) \tag{S14}$$

Equations (S13) and (S14) show that water evaporation is influenced by the combination of concrete's surface conditions (temperature and humidity on the surface) and ambient meteorological conditions (atmospheric temperature, wind speed, and humidity). For example, solar radiation will cause the surface temperature to rise, thereby increasing the water vapor pressure on the surface and increasing evaporation. These factors have been reflected by the boundary conditions of our model.

When the concrete surface is sprayed with water (free water), the surface is deemed as wet, and the relative humidity of the environment is taken as φ_e=100%. The water exchange is the transport of liquid water caused by the relative humidity difference at the boundary, and the flux density of water vapor diffusion g_w (kg/m^2 s) can be expressed as:

$$g_{\mathrm{w}} = D_s\left(1-\varphi_s\right) \tag{S15}$$

where: Ds is the relative humidity diffusion coefficient of the wet surface, which is generally taken as 10 D_1.

Section S6 Discussion on Creep Model

The early concrete creep vector includes the recoverable short-term creep $\boldsymbol{\varepsilon_{kv}}$ vector and the irrecoverable long-term creep $\boldsymbol{\varepsilon_{am}}$ vector. The one-dimensional model consists of a viscoelastic body and a viscous body in series to reflect the recoverable creep and non-recoverable creep of the early concrete respectively [45].

The one-dimensional model of short-term creep can be expressed as:

$$E_{kv}\left(\alpha\right)\left(\varepsilon_{kv}+\tau\dot{\varepsilon}_{kv}\right)=\sigma \tag{S16}$$

In addition to age effects, stress states such as tensile/compression state, stress level, and multi-axial stress behavior all affect the development of early creep.
(1) Influence of tension/compression state

In equation (S16), τ—relaxation time of viscoelastomer, research holds that 24h can satisfy the deformation of early concrete viscoelastic body; $E_{kv}(\alpha)$ —elastic modulus of viscoelastic body, which can be expressed as a function of hydration degree.

$$E_{kv}\left(\alpha\right)=E_{kv}^{\infty}\frac{0.473}{2.081-1.608\left(\dfrac{\alpha-\alpha_0}{\alpha_u-\alpha_0}\right)^{0.62}} \tag{S17}$$

In equation (S17), E_{kv}^{∞}—final elastic modulus of viscoelastic body, GPa.
The long-term creep of concrete is irreversible and can be simulated by viscous body related to its hydration degree. The one-dimensional creep can be expressed as:

$$\dot{\varepsilon}_{\mathrm{am}}=\frac{\sigma}{\eta_{am}\left(\alpha\right)} \tag{S18}$$

In equation (S18), the viscosity coefficient $\eta_{am}(\alpha)$ of the viscous body is a function of the equivalent age $t_{eq}(\alpha)$ related to hydration degree, expressed as:

$$\eta_{am}\left(\alpha\right)=\eta_{am}t_{eq}\left(\alpha\right) \tag{S19}$$

(1) Influence of tension/compression state

The creep law of early concrete under tensile and compressive conditions is different. At present, it is generally believed that tensile creep will lead to the development of microcracks in concrete, and the tensile creep caused by microcracks can not be recovered. Therefore, the influence of stretching/compression state on creep can be reflected by introducing the stretching/compression creep correction coefficient for irreversible creep [46].

$$\dot{\varepsilon}_{am} = \beta_{am} \frac{\langle \sigma \rangle_{+}}{\eta_{am}(\alpha)} + \frac{\langle \sigma \rangle_{-}}{\eta_{am}(\alpha)} \tag{S20}$$

In equation (S20), β_{am}—the correction factor for tensile/compressive creep of early concrete, which is generally greater than 1.0. In this paper, the reference [46] for track bed concrete sets the value as 1.6.

(2) Stress level influence

At present, most scholars believe that the early creep of concrete has nonlinear characteristics, that is, the greater the stress level, the greater the creep degree (the creep under 1MPa stress, $u\varepsilon$/MPa). Some scholars believe that only when the stress level is greater than a certain value (45% compression, 25% tensile), the creep shows nonlinear characteristics. Under high stress, the creep rate increases with time, and irreversible creep damage may occur. In this model, the nonlinear functional relationship between non-recoverable creep strain and stress $\boldsymbol{\sigma}$ under high stress is established, and the creep correction coefficient is adopted, expressed by stress level s as

$$\beta_{\sigma} = \frac{1+s^2}{1-s^{10}} \tag{S21}$$

$$s = \frac{\sigma}{f(\alpha)} \tag{S22}$$

In equation (S22), $f(\alpha)$—tensile/compressive strength at a hydration degree of α.

The relationship between creep correction coefficient and stress level obtained according to equation (S22) is shown in figure 2. As can be seen from the figure, when the stress level exceeds 0.8, the creep rate increases geometrically.

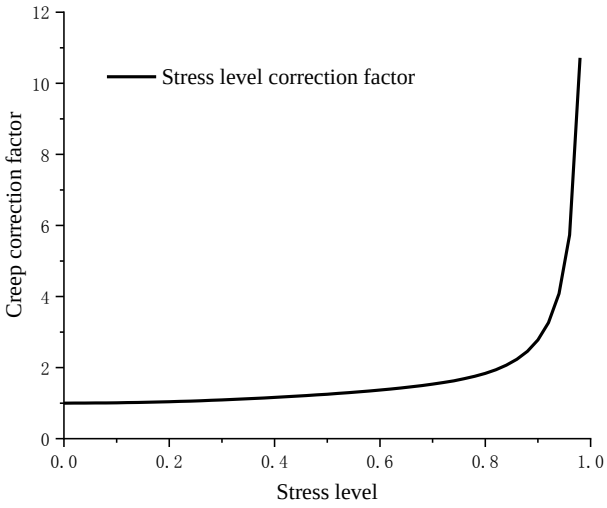

Fig. S2 Stress level correction factor

(3) Multi-axial force effect

Under the action of multi-axial stress, creep in different directions influences each other, resulting in obvious spatial characteristics of creep distribution in concrete structures. At present, the research on multi-axial creep is not mature, but by introducing the creep Poisson ratio νc, the empirical range of the creep Poisson ratio is 0.1~0.15 [47], and the value is set as 0.12 in this paper. The creep model after extending burgers's body to multi-axis state includes 12 variables, respectively 6 recoverable creep strains (ε_x^{kv}, ε_y^{kv}, ε_z^{kv}, ε_{xy}^{kv}, ε_{yz}^{kv}, ε_{xz}^{kv}) and 6 non-recoverable creep strains (ε_x^{am}, ε_y^{am}, ε_z^{am}, ε_{xy}^{am}, ε_{yz}^{am}, ε_{xz}^{am}).

Section S7 Numerical programs information, Model validation and calculation parameters

7.1 Numerical programs information

The slab used in the double-block track in subgrade sections adopts a longitudinal continuous cast-in-place structure, which experiences large temperature stress due to the strong longitudinal constraints, so it has a higher risk of cracking than the segmented unit slab used in bridge sections. Therefore, this paper selects the continuous track slab used in subgrade sections for modeling.

Construction tool rails and fasteners are used to precisely position the sleepers before pouring concrete. To prevent the thermal expansion and contraction of the tool rails from causing adverse effects on the early-age track bed, they are removed after initial setting and before the concrete fully sets, so that the stress of the early-age concrete will not be affected. For this reason, the tool rails and fasteners are not considered in our model.

The double-block sleeper is embedded in the cast-in-place concrete of the track bed, causing sudden changes in the structure and material properties of the concrete at the sleeper position and causing drastic changes in the temperature, humidity, and mechanical fields of the track bed at areas near the sleeper. A large number of on-site investigations have also found that most cracks in

the track bed occur near the sleeper's position, which suggests a close relationship between the track bed's cracking and the sleeper, proving the sleeper's importance to the model. It must be noted that the concrete sleeper is prefabricated in the factory, which means that when the concrete of the track bed is poured on-site, the concrete of the sleeper is already hydrated and matured, and this hydration field is constant and does not change over time. The concrete supporting layer below the track bed restrains the displacement of the track bed to a certain extent, so it is also closely related to the cracking of the track bed and thus should be considered when modeling. Similar to the sleeper, the supporting layer is poured in advance and has been fully hydrated and matured at the time of pouring the track bed, and therefore the hydration field in the supporting layer is also regarded as a constant.

In the calculation model, the temperature field and the temperature effect, the humidity field and the humidity effect on the bonding surface between the early track bed concrete and the mature concrete of the sleeper and support layer are treated as the fourth type of boundary conditions, that is, the temperature and heat flow, relative humidity and humidity flux on the contact surface are continuous. The force field coupling at the joint surface is treated as binding contact, that is, displacement continuity.

Mature sleepers and supporting layers are divided into 4,368 hexahedral units. There are six variables of fields, namely hydration (variable: degree of hydration α), temperature (variable: temperature T), humidity (variable: relative humidity φ), and force (variables: displacements in three directions u, v, and w). They are expressed by second-order Lagrangian interpolation functions, with a total of 185,640 degrees of freedom.

The track bed is divided into 5,392 hexahedral units. There are six variables, namely the hydration field (variable: degree of hydration α), temperature field (variable: temperature T), humidity field (variable: relative humidity φ), mechanical field (variables: displacements in three directions u, v, and w), which are expressed by second-order Lagrangian interpolation functions.

It total, there are 12 variables to describe creep in the mechanical field, namely ε_x^{kv}, ε_y^{kv}, ε_z^{kv}, ε_x^{kv}, ε_y^{kv}, ε_{xz}^{kv}, ε_x^{am}, ε_y^{am}, ε_z^{am}, ε_{xy}^{am}, ε_{yz}^{am}, and ε_{xz}^{am}. The first-order Lagrangian shape function is used, with a total of 352,636 degrees of freedom.

7.2 Model validation

The reliability of the model is systematically verified by test data of various load conditions, but this is not covered in this paper. We only focus on the applicability of the model for predicting stress development of early-age concrete structures under the constraint state. Fig. S3 shows the comparison of the early-age concrete constraint stress test conducted by Li [59] with the stress development results obtained from our mechanical field calculation.

The constraint stress of concrete was first in the state of compression and then into tension, with the maximum compressive stress of 0.45 MPa reached at hour 24. The prediction results of the model show a good agreement with the test results, indicating our model can predict the stress development of early-age concrete.

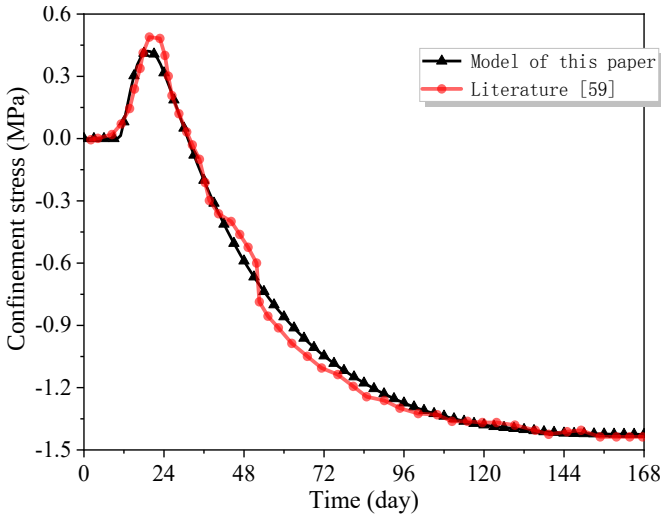

Fig. S3 Early-age concrete confinement stress verification

7.3 Calculation parameters

The numerical calculations used in this model, including the main calculation parameters for the track bed, supporting layer, and sleepers are shown in Tables 1, 2, and 3, respectively.

Table S1. Calculation parameters of track bed

Parameter	Unit	Value
B_1	1/h	0.9
B_2	-	7×10^{-4}
η	-	6.0
e	-	8.0
E_a	KJ/mol	45.0
α_u	-	0.78
Q_h^∞	kJ/kg	430
C_a	kJ/(kg·K)	0.8
C_c	kJ/(kg·K)	0.85
C_{cp}	kJ/(kg·K)	0.72
C_w	kJ/(kg·K)	4.187
λ_c	W/(m·K)	1.3
λ_w	W/(m·K)	0.6
λ_a	W/(m·K)	3.3
f_w	-	7.0
Q_w^∞	-	0.25
w_{f0}	kg/m^3	170
w_{fu}	kg/m^3	105
b_0	-	1.02
n_b	-	0.005
m_b	-	10
D_1^∞	m^2/h	
φ_c	-	0.8
n_φ	-	15
n_D	-	8.0
μ_0	-	40
n_μ	-	5.0
α_0	-	0.2
E	GPa	32.5
f_t	MPa	2.39
β_E	-	0.6
β_t	-	1.0
v	-	0.2
α_T	1/℃	1×10^{-5}

Parameter	Unit	Value
α_{φ}	1/%	1×10^{-5}
E_{kv}^{∞}	GPa	90
τ	h	24.0
η_{am}	GPa	400
v_c	-	0.12

Table S2. Calculation parameters of supporting layer

Parameter	Unit	Value
b	-	1.2
w_{fu}	(kg/m^3)	130
λ_{dry}	(W/m K)	1.2
C_{dry}	kJ/(kg K)	1.05
D_1	(m s^{-2})	8×10^{-6}
φ_c	-	0.8
n_{φ}	-	15
E	GPa	28.5
v	-	0.2
α_T	1/℃	1×10^{-5}
α_{φ}	/%	1×10^{-5}

Table S3. Calculation parameters of sleepers

Parameter	Unit	Value
b	-	1.1
w_{fu}	(kg/m^3)	90
λ_{dry}	(W/m K)	1.5
C_{dry}	kJ/(kg K)	0.9
D_1	(m s^{-2})	8×10^{-7}
φ_c	-	0.8
n_{φ}	-	10
E	GPa	35.5
v	-	0.2
α_T	1/℃	1×10^{-5}
α_{φ}	1/%	1×10^{-5}

Section S8 Discussion of the importance of creep

As an important property of early concrete, creep has the effect of relaxing the restraint stress of track bed. Under the influence of environment, the temperature difference between day and night in the flat structure of track bed is large, and the early creep is more complicated under the alternating action of tension and compression. Existing studies have not considered the early creep deeply enough. This paper studies the influence of creep on the early cracking mechanism of the track bed by comparing whether the calculation results of creep are considered or not. In this paper, the time-history data of crack risk at track bed points 1~3 are calculated under two conditions: considering creep and not considering creep. The results are plotted as shown in the figure. As shown in the figure, creep can effectively reduce the risk of early track bed cracking, and the influence of creep on cracking risk increases as the age increases. By the 7th day after casting, the impact of creep on cracking risk reaches 50%. Among them, when considering the creep within 7 days, the cracking risk of surface point 1 is the highest, and when not considering the creep, the cracking risk of plate bottom point 3 is the highest. This is because the plate bottom is subject to the bonding constraint of the support layer, and its constraint degree and creep effect are stronger than those of the plate middle and surface. It can be seen that creep plays an important role in stress development of early track concrete, so creep should be considered in early track cracking

risk assessment.

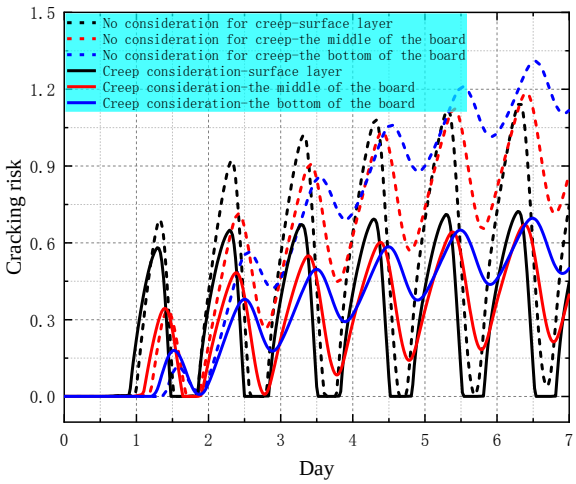

Fig. S4 Consider the effect of creep or not on the risk of cracking

Section S9 The calculation details and cracking risk analysis of each influence condition

9.1 Impact of material properties of concrete and control measures

9.1.1 Impact of maximum heat of hydration and control measures

This subsection investigates cracking in the early-age concrete track bed with different maximum heats of hydration in cement, including 480 kJ/kg (rapid-hardening cement), 430 kJ/kg (ordinary Portland cement), and 380 kJ/kg (low-heat cement), respectively. The variation of the maximum risk coefficient with the maximum heat of hydration for each layer of the track bed is shown in Fig. S5.

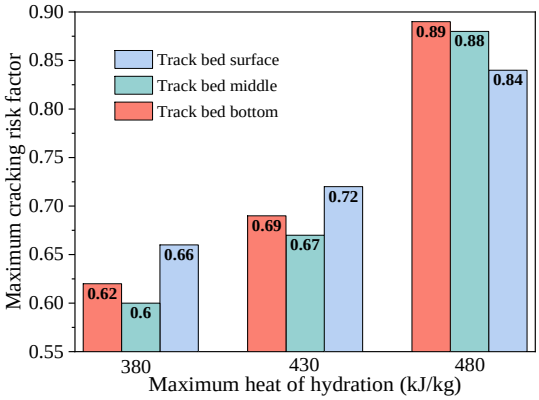

Fig. S5 Variation of risk of cracking of the track bed with different heats of hydration

In Fig. S5, the increase of the maximum heat of hydration shows rapid growth in the risk of cracking of each layer of the concrete track bed (upper concave curves). When the maximum heat of hydration exceeds 430 kJ/kg, the maximum risk of cracking of the surface layer reaches 0.72, which exceeds the cracking risk coefficient control threshold of 0.7. Therefore, in engineering projects, the maximum heat of hydration of the track bed concrete should not exceed 430 (kJ/kg).

In modern construction, especially for the O&M of high-speed slab tracks, rapid-hardening concrete is typically used thanks to the benefits in strength and rapid development. However, since using rapid-hardening concrete can lead to a great risk of cracking, it is recommended to be cautious and only use rapid-hardening concrete where necessary.

9.1.2 Influence of heat release peak time (hydration rate) and control measures

In this subsection, we analyze the influence of three types of concrete (fast hardening cement, reference cement, and delayed setting cement) with different heat release peak times on the risk of early-age cracking of the track bed. These hydration processes can be simulated by changing the hydration affinity potential coefficients. The affinity potential coefficients and the corresponding heat release peak time and maximum hydration rates are shown in Table S4. The corresponding risks of cracking in the concrete track bed at different heat release peak times are shown in Fig. S6.

Table S4 Hydration rate parameters

Parameter	Fast hardening cement	Reference cement	Delayed setting cement
B_1	0.5	1.0	1.5
B_2	7×10^{-4}	7×10^{-4}	7×10^{-4}
η	4	6	5.5
Maximum hydration rate	0.68/day	0.8/day	1.35/day
Maximum heat release time	15h	7h	5h

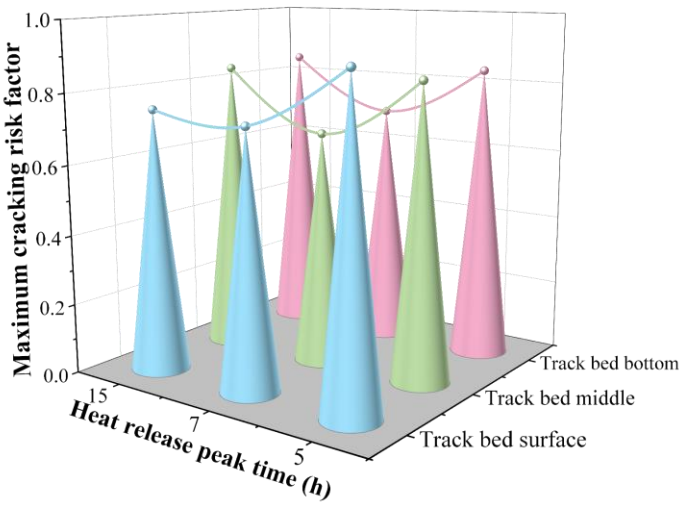

Fig. S6 Variation of the risk of cracking in the concrete track bed with different heat release peak time

Fig. S6 shows the impact of the heat release peak time on the possibility of cracking in the concrete track bed, and the influence of the maximum heat release peak time as an upward concave function. Too fast or too slow a hydration process will significantly increase the risk of cracking. To effectively reduce the cracking risk of early-age concrete track beds, we must control the heat release peak time of concrete, with an optimal heat release peak time at about nine hours after pouring, which is similar to the final setting time of early-age concrete.

9.2 Impact of atmospheric factors in construction environment and control measures

9.2.1 Influence of temperature difference between day and night and control measures

To investigate the difference of temperature between day and night on the early-age concrete track bed cracking, we set the temperature difference between day and night as 6 ℃, 12 ℃, and 18 ℃. Their influence on the risks of cracking of the track bed is shown in Fig. S7.

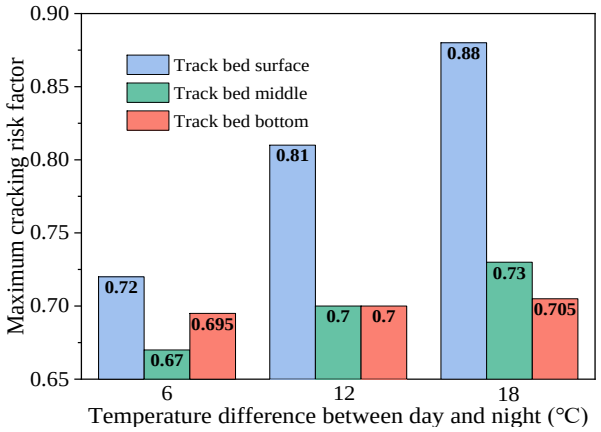

Fig. S7 Variation of track bed cracking risks with different temperature differences between day and night

We can see that the risk of cracking increases with large differences in temperature between day and night, and the maximum cracking risk coefficient of the track bed shows a positive linear correlation with the temperature difference between day and night; further, the closer to the surface of the track bed, the more the risk of cracking to the track bed caused by differences in temperature. When this difference is 18 ℃, the maximum cracking risk of the track bed slab surface is nearly 0.9, indicating a high risk of cracking on the track bed surface.

To reduce the risk of cracking of early-age concrete track beds, pouring should be avoided in weather that experiences large temperature changes in the daytime and nighttime; otherwise, the newly poured concrete should be insulated to minimize the impact of the temperature.

9.2.2 Effect of daily average cooling rate and control measures

We set the average daily cooling values as 0.25 ℃/day, 0.5 ℃/day, and 0.75 ℃/day within 7 days since the concrete was cast into the mold and calculated the cracking risk of the track bed at different cooling rates. The results are shown in Fig. S8.

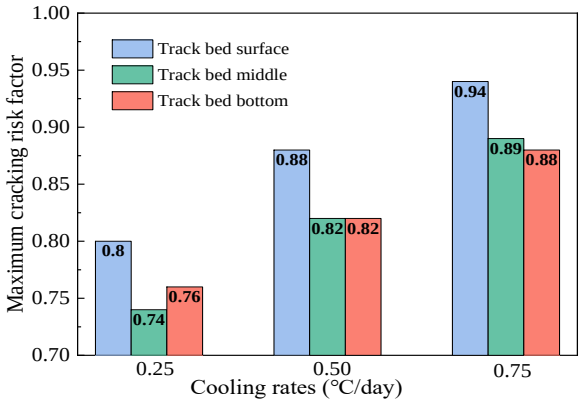

Fig. S8 Variation of maximum cracking risk of each layer of the track bed at different cooling rates

As can be seen from Fig. S8, we can see that faster cooling rates correspond to a greater risk of cracking. This relationship is near linear, and the cooling rate has basically the same effect on the cracking risk at different depths. When the cooling rate is 0.75 ℃/day, the cracking risk coefficient of the surface layer reaches up to 0.94, and the value also reaches 0.89 and 0.88 at the middle and bottom of the slab, indicating a greater risk of cracking. From this, we know that continuous cooling weather after casting can cause great cracking risk to the whole early-age track bed, the pouring of track bed slabs should be avoided during cold weather.

9.2.3 Effect of solar radiation intensity and control measures

We take the maximum intensity of solar radiation Q_{∞}^{max} as 800, 600, and 400 (W/m^2 ℃), to calculate the risks of track bed cracking at different solar radiation intensities (Fig. S9).

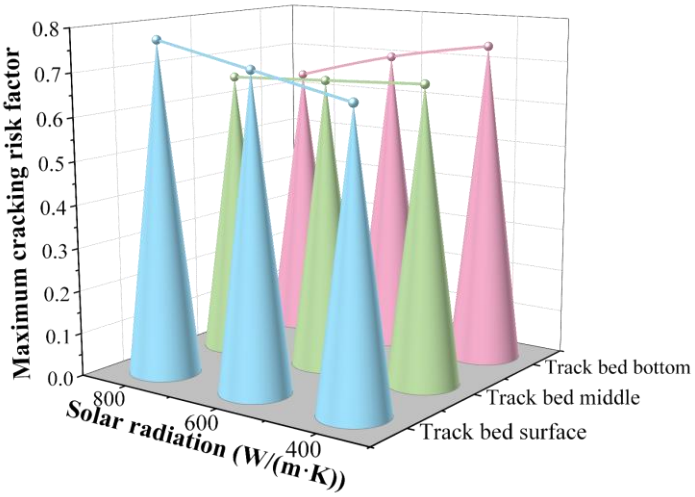

Fig. S9 Variation of cracking risks of each layer of track bed with different solar radiation intensities

The solar radiation in Fig. S9 shows different patterns on the cracking risk of the surface, middle, and bottom layers of the track bed. We can see the cracking risk of the surface layer has a positive linear relationship with the solar radiation intensity, but the risk of cracking at the middle and bottom layers shows a negative linear relationship with the solar radiation intensity. When the

solar radiation is 800 (W/m^2 K), the cracking risk of the surface layer is about 0.77, indicating a high risk of cracking. It should be noted that when studying the effect of solar radiation, the calculations are performed under the curing condition of standard geotextile covering early-age concrete track bed (the solar radiation coefficient of track bed surface being 0.2), so the solar radiation intensity in this study is not the real solar radiation absorbed by the track bed surface. That is, the risk of cracking will increase by many times if the exposed track bed surface is not protected by sunscreen treatment.

Covering the surface of the track bed after pouring is important to reduce the risk of cracking. From Fig. S7, we see that even with the current standard surface covering treatment, there is still a risk of cracking on the surface, making it necessary to further enhance the existing covering measures.

9.3 Impact of construction techniques and control measures

9.3.1 Influence of molding temperature and control measures

Fig. S10 shows the molding temperatures set as 10, 15, and 20 ℃ respectively and the impact of different molding temperatures on the risk of track bed cracking.

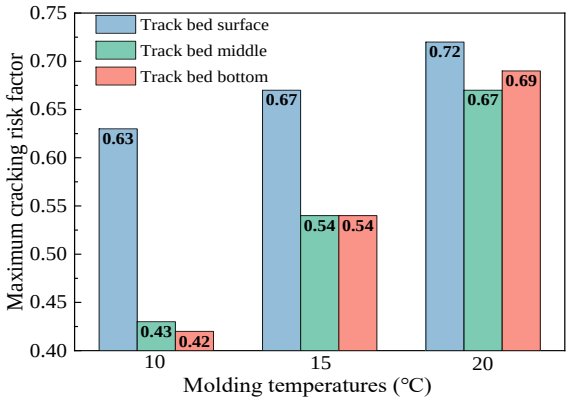

Fig. S10 Variation of cracking risk of each layer of the track bed at different molding temperatures

In Fig. S10, we see the risk of cracking increases linearly with the rise in molding temperature, which has a significantly higher impact on the middle and bottom layers that are less affected by ambient temperature. When the molding temperature rises to 20 ℃, the risk coefficient of cracking on the surface has exceeded the limit value of 0.7, indicating a high risk of cracking.

From this we can ascertain that a suitable (not too high) concrete molding temperature can mitigate the risk of cracking. It should be noted that the influence law is applicable to only the construction environment and atmosphere conditions set in this study. In winter seasons when the ambient temperature is too low, a lower molding temperature may lead to the low hydration rate and slow strength growth and increase the possibility of cracking. The relationship between cracking risk and molding temperature in different seasons needs to be further studied.

9.3.2 Influence of the molding time and control measures

This study sets the molding time at 4:00, 12:00, and 20:00 to analyze the influence of different molding times on the cracking risk of the track bed. The results are shown in Fig. S11.

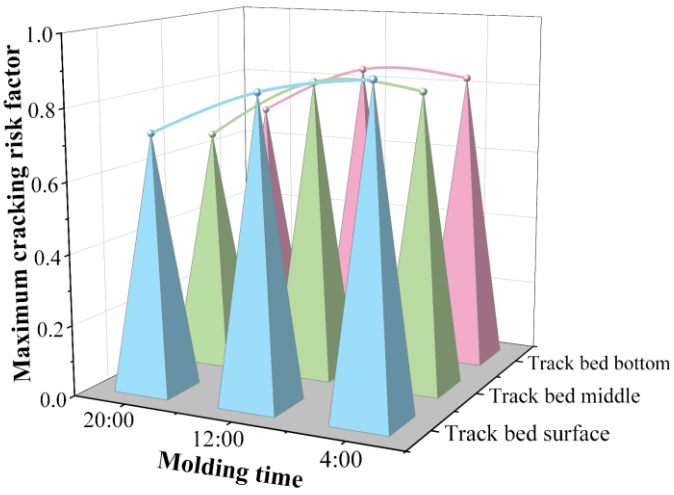

Fig. S11 Variation of cracking risk of each layer of track bed with different molding time

From Fig. S11, it can be seen that the track bed molded at around 04:00 has the highest risk of surface cracking (maximum cracking risk factor of 0.9), while the track bed molded at around 10:00 has the highest risk of cracking in the middle and bottom layers of the slab (maximum cracking risk factor of 0.85). The track bed molded at around 20:00 has the lowest risk of cracking.

We can determine that an appropriate molding time can positively control the risk of cracking in the track bed, and the optimal molding time is around 20:00.

9.3.3 Influence of insulation coefficient and control measures

During the construction of the double-block ballastless tracks, different maintenance methods are used to fit various site conditions, and these maintenance methods can influence the risk of cracking in the track bed. This paper defines the insulation coefficient of the thermal insulation material Θ as:

$$\Theta=\frac{\left(a_{v,\ l}-a_{v,\ b}\right)}{a_{v,\ l}} \tag{S23}$$

where: $a_{v,l}$ refers to the convective heat transfer coefficient when the surface layer of the track bed is exposed; and $a_{v,b}$ is the equivalent convection heat transfer coefficient when the track bed is covered with insulation. The insulation coefficients are set as 0.25, 0.5, and 0.75 respectively, the results of which on the risk of cracking of the track are calculated (Fig. S12).

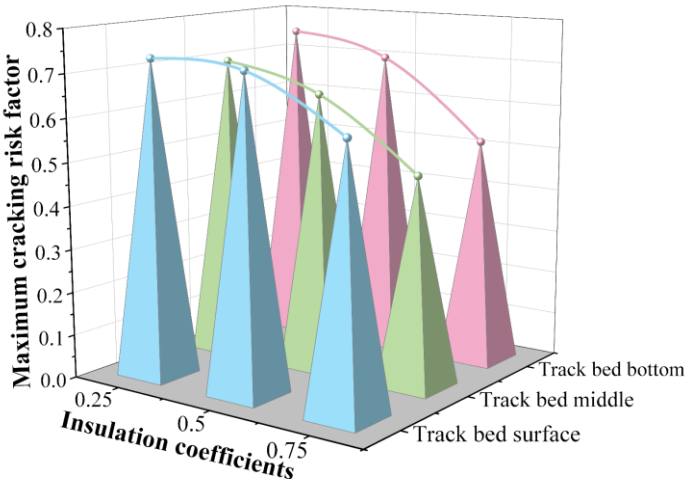

Fig. S12 Variation of cracking risks in each layer of track bed with different insulation coefficients

Fig. S12 shows that the cracking risk of the track bed and the insulation coefficient are in an upward convex functional relationship, and the insulation layer can effectively reduce the risk of cracking of the surface layer only when the insulation coefficient is higher than 0.5. Therefore, under conditions of unfavorable ambient temperatures, strong insulation must be used after the concrete is poured to minimize cracking in the track bed's surface layer.

References

[1] Ren JJ, Yang RS, Wang P, Yong P, Wen C, Slab upwarping of twin-block slab track on subgrade-bridge transition section parameter study and repair method, Transport. Res. Rec. (2014) 115-124.https://doi.org/10.3141/2448-14.

[2] K Scrivener, A Ouzia, P Juilland, AK Mohamed, Advances in understanding cement hydration mechanisms. Cem. Concr. Res. 124(2019). https://doi.org/10.1016/j.cemconres.2019.105823.

[3] M Cervera, R Faria, J Oliver, T Prato, Numerical modelling of concrete curing, regarding hydration and temperature phenomena. Comput. Struct. 80(2002) 1511-1521. https://doi.org/10.1016/S0045-7949(02)00104-9.

[4] D Gawin, F Pesavento, B A Schrefler. Hygro-thermo-chemo-mechanical modelling of concrete at early ages and beyond Part I: Hydration and hygro-thermal phenomena. Int. J. Numer. Meth. Eng. 67(2006) 332-363. https://doi.org/10.1002/nme.1636.

[5] DI LUZIO G, G Cusatis. Hygro-thermo-chemical modeling of high performance concrete I: Theory. Cem. Concr. Compos. 31(2009) 309-324.

[6] R Krstulovic, P. A Dabic, conceptual model of the cement hydration process. Cem. Concr. Res. 30(2000) 693-698. https://doi.org/10.1016/S0008-8846(00)00231-3.

[7] Yan PY, Zheng F. Review on hydration of composite cementitious materials, Guisuanyan Xuebao. 45(2007) 1066-1072. https://doi.org/ 10.14062/j.issn.0454-5648.2017.08.03.

[8] HJH Brouwers, DE Korte, Multi-cycle and multi-scale cellular automata for hydration simulation (of Portland-cement), Comput. Mater. Sci. 111(2016) 116-124. https://doi.org/10.1016/j.commatsci.2015.08.049.

[9] J.W. Bullard, A three-dimensional microstructural model of reactions and transport in aqueous

mineral systems, Modell. Simul. Mater. Sci. Eng. 15(2007) 711-738. https://doi.org/10.1088/0965-0393/15/7/002.
[10] K. van Breugel, Numerical-simulation of hydration and microstructural development in hardening cement-based materials .2. applications. Cem. Concr. Res. 25(1995) 522-530. https://doi.org/10.1016/0008-8846(95)00041-A.
[11] K. van Breugel, Numerical simulation of hydration and microstructural development in hardening cement-based materials (I) theory, Cem. Concr. Res. 25(1995) 319-331. https://doi.org/10.1016/0008-8846(95)00017-8.
[12] S. Bishnoi, K L. Scrivener, uic: A new platform for modelling the hydration of cements, Cem. Concr. Res. 39(2009) 266-274. https://doi.org/10.1016/j.cemconres.2008.12.002.
[13] Wu SX, Huang DH, Lin FB, Zhao HT, Wang PX, Estimation of cracking risk of concrete at early age based on thermal stress analysis, J. Therm. Anal. Calorim. 105(2011) 171-186. https://doi.org/10.1007/s10973-011-1512-y.
[14] Zhang J, Gao Y, Han YD, Sun W, Shrinkage and Interior Humidity of Concrete under Dry-Wet Cycles, Dry. Technol. 30(2012) 583-596. https://doi.org/10.1080/07373937.2011.653614.
[15] Ba HJ, Su AS. Gao XJ, Qi T., Cracking tendency of restrained concrete at early ages, J. Wuhan. Univ. Technol. 23(2008) 263-267. https://doi.org/10.1007/s11595-006-2263-7.
[16] R. Combrinck, L. Steyl, W.P. Boshoff, Interaction between settlement and shrinkage cracking in plastic concrete, Constr. Build. Mater. 185(2018) 1-11. https://doi.org/10.1016/j.conbuildmat.2018.07.028.
[17] Liu JP, Tian Q, Wang YJ, Li H, Xu W, Evaluation method and mitigation strategies for shrinkage cracking of modern concrete, Engineering-PRC. 7(2021) 348-357. https://doi.org/10.1016/j.eng.2021.01.006.
[18] Du MY, Jin XY, Ye HL, Jin NG, Tian Y, A coupled hygro-thermal model of early-age concrete based on micro-pore structure evolution, Constr. Build. Mater. 111(2016) 689-698. https://doi.org/10.1016/j.conbuildmat.2015.10.187.
[19] Zhou W, Qi TQ, Liu XH, Feng CQ, Yang SH, A hygro-thermo-chemical analysis of concrete at an early age and beyond under dry-wet conditions based on a fixed model, Int. J. Heat Mass Transfer. 115(2017) 488-499. https://doi.org/10.1016/j.ijheatmasstransfer.2017.08.014.
[20] Zhou W, Qi TQ, Liu XH, Yang SH, Feng CQ, A meso-scale analysis of the hygro-thermo-chemical characteristics of early-age concrete, Int. J. Heat Mass Transfer. 129(2019) 690-706. https://doi.org/10.1016/j.ijheatmasstransfer.2018.10.001.
[21] H.W. Park, D.H. Kim, J.S. Lim, C.S. Shim, J.H. Jeong, Prediction of differential drying shrinkage of airport concrete pavement slabs, Int. J. Pavement Eng. 22(2021) 752-762. https://doi.org/10.1080/10298436.2019.1645847.
[22] Xu GD, Tian Q, Miao JX, Liu JP, Early-age hydration and mechanical properties of high volume slag and fly ash concrete at different curing temperatures, Constr. Build. Mater. 149(2017) 367-377. https://doi.org/10.1016/j.conbuildmat.2017.05.080.
[23] Gao Y, Zhang J, Han P, Determination of stress relaxation parameters of concrete in tension at early-age by ring test, Constr. Build. Mater. 41(2013) 152-164. https://doi.org/10.1016/j.conbuildmat.2012.12.004.
[24] Hou DW. Study on the integration of concrete itself and drying shrinkage and related problems. MS Thesis, Tsinghua university, Beijing, China (in Chinese).
[25] Zhang J, Hou DW, Gao Y, Uniform driving force for autogenous and drying shrinkage of

concrete, Qinghua Daxue Xuebao, Ziran Kexueban. 50(2010) 1321-1324. https://doi.org/10.16511/j.cnki.qhdxxb.2010.09.015.
[26] Jiang YB, Zhou H, Beer M, Wang L, Zhang JR, Zhao LJ, Robustness of load and resistance design factors for rc columns with wind-dominated combination considering random eccentricity, J. Struct. Eng. 143(2017). https://doi.org/10.1061/(ASCE)ST.1943-541X.0001720.
[27] G. De Schutter, L. Taerwe, Degree of hydration-based description of mechanical properties of early age concrete, Mater. Struct. 29(1996) 335-344. https://doi.org/10.1007/BF02486341.
[28] Xiong XY, Wang LJ, Creep law of self-compacting concrete, Mater. Res. Innovations. 19(2015) 739-743. https://doi.org/10.1179/1432891714Z.0000000001185.
[29] M.H. Hubler, R. Wendner, Z.P. Bazant, Statistical justification of Model B4 for drying and autogenous shrinkage of concrete and comparisons to other models, Mater. Struct. 48(2015) 797-814. https://doi.org/10.1617/s11527-014-0516-z.
[30] D. Gawin, F. Pesavento, B.A. Schrefler, Hygro-thermo-chemo-mechanical modelling of concrete at early ages and beyond. Part I: Hydration and hygro-thermal phenomena, Int. J. Numer. Meth. Eng. 67(2006) 299-331. https://doi.org/10.1002/nme.1615.
[31] Liu XH, Zhou CB, Chang XL, Zhou W, Simulation of temperature crack propagation considering nonlinear creep of concrete, Yantu Lixue. 31(2010) 1995-2000,2005. https://doi.org/10.16285/j.rsm.2010.06.031.
[32] Hai DF, ZHONG FX, Nonlinear creep analysis method for concrete structures, Engineering Mechanics. 31(2014) 96-102. https://doi.org/10.6052/j.issn.1000-4750.2012.09.0685.
[33] F. Benboudjema, F. Meftah, J.M. Torrenti, Interaction between drying, shrinkage, creep and cracking phenomena in concrete, Eng. Struct. 27(2005) 239-250. https://doi.org/10.1016/j.engstruct.2004.09.012.
[34] Z.P. Bažant, Prediction of concrete creep and shrinkage: past, present and future, Nucl. Eng. Des. 203(2001) 27-38. https://doi.org/10.1016/S0029-5493(00)00299-5.
[35] Du MY, Jin XY, Ye HL, Jin NG, Tian, Y, A coupled hygro-thermal model of early-age concrete based on micro-pore structure evolution, Constr. Build. Mater. 111(2016) 689-698. https://doi.org/10.1016/j.conbuildmat.2015.10.187.
[36] You WJ, Zhang FP, Huang Y, Gao M, Wen CQ, Yang GT, A coupled hygro-thermo-mechanical model for the evolution of saturation in early-age concrete, Int. J. Heat Mass Transfer. 156(2020). https://doi.org/10.1016/j.ijheatmasstransfer.2020.119817.
[37] M. Bocciarelli, G. Ranzi, Identification of the hygro-thermo-chemical-mechanical model parameters of concrete through inverse analysis, Constr. Build. Mater. 162(2018) 202-214. https://doi.org/10.1016/j.conbuildmat.2017.11.167.
[38] Luzio G D , Cusatis G .Hygro-thermo-chemical modeling of high-performance concrete. II: Numerical implementation, calibration, and validation[J].Cement & Concrete Composites, 2009, 31(5):309-324. https://doi.org/10.1016/j.cemconcomp.2009.02.016.
[39] Lin F, Meyer C. Hydration kinetics modeling of portland cement considering the effects of curing temperature and applied pressure[J]. Cement & Concrete Research. 2009, 39(4): 255-265. https://doi.org/10.1016/j.cemconres.2009.01.014.
[40] Liu JP, Tian Q. Early-age deformation and shrinkage crack control of modern concrete [M]. Science Press ,2020.
[41] Künzel H M. Simultaneous heat and moisture transport in building components. One-and two-dimensional calculation using simple parameters[J]. JRB Verlag. 1995.

[42] Zhu Bofang. Thermal stresses and temperature control of mass concrete. Tsinghua University Press, 2014.
[43] Yang SJ, Cheng C, Bao Q, Zhong Y, Inverse calculation of absorption coefficient of concrete with heat-reflective coating on surface, Forest Engineering. 35(2019) 87-92 https://doi.org/10.16270/j.cnki.slgc.2019.02.014.
[44] Huo XS, Wong LU, Experimental study of early-age behavior of high performance concrete deck slabs under different curing methods, Constr. Build. Mater. 20(2006) 1049-1056. https://doi.org/10.1016/j.conbuildmat.2005.04.001.
[45] Schutter G D. Degree of hydration based Kelvin model for the basic creep of early age concrete[J]. Materials & Structures. 1999, 32(4): 260-265. https://doi.org/10.1007/BF02479595.
[46] Briffaut M, Benboudjema F, Torrenti J, et al. Concrete early age basic creep: Experiments and test of rheological modelling approaches[J]. CONSTRUCTION AND BUILDING MATERIALS. 2012, 36: 373-380. https://doi.org/10.1016/j.conbuildmat.2012.04.101.
[47] LI SW. Study on time–depending structural behavior of long-span cantilever casting pc box girder bridges based on thermo–hydro–mechanical combined effects analysis [D]. Southwest Jiaotong University, 2019.
[48] Li, Fei, Qin WZ, Restraint stress and stress relaxation in concrete at early ages, Qinghua Daxue Xuebao, Ziran Kexueban. 50(2010) 363-366. https://doi.org/10.16511/j.cnki.qhdxxb.2010.03.022.